

Resonance inversion in a superconducting cavity coupled to artificial atoms and a microwave background

Juha Leppäkangas,¹ Jan David Brehm,¹ Ping Yang,¹ Lingzhen Guo,²
Michael Marthaler,^{3,4} Alexey V. Ustinov,^{1,5} and Martin Weides^{1,6}

¹*Physikalisches Institut, Karlsruhe Institute of Technology, 76131 Karlsruhe, Germany*

²*Max Planck Institute for the Science of Light, 91058 Erlangen, Germany*

³*Institut für Theorie der Kondensierten Materie,*

Karlsruhe Institute of Technology, 76131 Karlsruhe, Germany

⁴*Theoretische Physik, Universität des Saarlandes, 66123 Saarbrücken, Germany*

⁵*Russian Quantum Center, National University of Science and Technology MISIS, 119049 Moscow, Russia*

⁶*School of Engineering, University of Glasgow, Glasgow G12 8QQ, UK*

We demonstrate how heating of an environment can invert the line shape of a driven cavity. We consider a superconducting coplanar cavity coupled to multiple artificial atoms. The measured cavity transmission is characterized by Fano-type resonances with a shape that is continuously tunable by bias current through nearby (magnetic flux) control lines. In particular, the same dispersive shift of the microwave cavity can be observed as a peak or a dip. We find that this Fano-peak inversion is possible due to a tunable interference between a microwave transmission through a background, with reactive and dissipative properties, and through the cavity, affected by bias-current induced heating. The background transmission occurs due to crosstalk with the multiple control lines. We show how such background can be accounted for by a Jaynes- or Tavis-Cummings model with modified boundary conditions between the cavity and transmission-line microwave fields. A dip emerges when cavity transmission is comparable with background transmission and dissipation. We find generally that resonance positions determine system energy levels, whereas resonance shapes give information on system fluctuations and dissipation.

I. INTRODUCTION

A Fano resonance [1] is a fundamental effect of wave propagation. It appears in a wide range of physical systems, including light propagation in photonic devices [2], charge transport in nanoelectronics [3], and inelastic scattering of elementary particles [1]. The Fano resonance emerges due to an interference effect between two parallel paths connecting input and output scattering states: Transmission through a continuous-mode or wide background state and transmission through a discrete or narrow energy-level. The resulting resonance can be both admitting or reflecting (anti-resonance) depending on the system details. As many other interference effects, it has numerous practical applications in metrology and optical engineering [2, 3].

In microwave devices, wanted or unwanted Fano-type resonances can easily emerge, for example, from capacitive or inductive background coupling between different ports of a resonant circuit [4]. In state-of-the-art superconducting quantum-microwave devices [5–8], a large number of qubits with control lines may need to be integrated into a small-sized chip, with possible further size-optimization to reduce decoherence sources, such as non-equilibrium quasiparticles [9] or field focusing [10]. In particular, a quantum-state measurement in these circuits is commonly based on microwave transmission through a readout resonator in a dispersive coupling regime [11]. When increasing circuit complexity and scaling up qubit numbers, it is difficult to avoid multiple interference paths for microwave signals propagating through the circuit. It is then of high interest to under-

stand in detail how Fano resonances can appear in such situations and how to account for them in most commonly used theoretical models.

In this article, we investigate microwave transmission across a superconducting coplanar cavity coupled to multiple superconducting artificial atoms. The measured transmission is characterized by Fano-type resonances with a shape that turns out to be continuously tunable by current bias through nearby flux control lines. In particular, we observe that the very same dispersive shift of the cavity, depending on the bias, can be seen as either a peak or a dip. We study the observed phenomena detailed further by establishing a theoretical model for cavity transmission in the presence of a microwave background. The background transmission accounts for a crosstalk between the input and output transmission lines through control lines bypassing the coplanar microwave cavity. We find that the well-known Jaynes- and Tavis-Cummings models [12–14] of the cavity-atom interaction are valid also for the considered system. The background transmission can be accounted for by modified boundary conditions between the cavity and transmission-line microwave fields.

Using the model, we study theoretically interference effects between microwave propagation beside and through the cavity. We find that dissipation and incoherent transitions strongly affect the observed line shape. For low drive powers and a weak coupling through the background, a change from a peak to a dip, which we call here a resonance inversion, is possible through an interplay between a background microwave transmission with reactive and dissipative properties, and a cavity transmission

with dissipative or incoherent dynamics. Essential is the comparison between the cavity transmission, background transmission, and background dissipation. All these contributions have to be of similar magnitude. A similar peak to dip transition can also emerge from other phenomena reducing the cavity transmission, such as photon blockade when increasing drive power [15–17]. Such higher drive amplitudes can have applications for quantum sensors [18] or quantum simulation [19, 20].

Based on theoretical results we explain the observed experimental features as an interplay between bias-induced heating and background transmission. The applied DC bias currents cause local heating of the bias leads, which in turn induce incoherent energy-level transitions in the cavity-atom system. Increasing rates of such transitions, by increasing the bias currents, reduces the cavity transmission and smoothly changes the spectroscopic response of the device from a peak to a dip, the latter appearing when the cavity transmission becomes comparable with the background transmission and dissipation. This allows for the full tunability of the Fano resonance shape. A similar phenomenon is also observed when directly increasing the (global) base temperature and when increasing the drive power [17].

The article is organized as follows. In Sec. II, we introduce our model of microwave scattering by a coplanar cavity. We show how microwave propagation beside the cavity can be included by additional terms in the boundary conditions. In Sec. III, we do a detailed analysis of the form of the Fano resonance under dissipation and decoherence. We show how the line shape of a microwave resonator can change from a peak to a dip under different conditions. In Sec. IV, we present our experimental results and analyze them with the established theory. Conclusions and discussion are given in Sec. V.

II. SYSTEM AND MODEL

The system we consider is shown in Fig. 1. Microwaves propagate in two semi-infinite transmission lines (TLs). The TLs are connected to each other through a two-sided cavity, described by coupling capacitors C_c and a resonant element Z . A direct coupling between the TLs (background) is provided by a parallel impedance Z_b . Multiple superconducting artificial atoms (transmons) are embedded in the cavity, affecting its resonance frequency.

We start building a theoretical model for this circuit in Sec. II A by introducing a quantized model of microwave radiation in TLs. In Sec. II B, we account for the coupling with the cavity-transmon system and in Sec. II C show how the parallel transmission channel can be included in the model by additional terms in microwave boundary conditions. A full solution in the linear limit is derived in Sec. II D and dissipation and fluctuations due to finite temperature are considered in Sec. II E. A linear scattering model, where all the circuit elements are described as

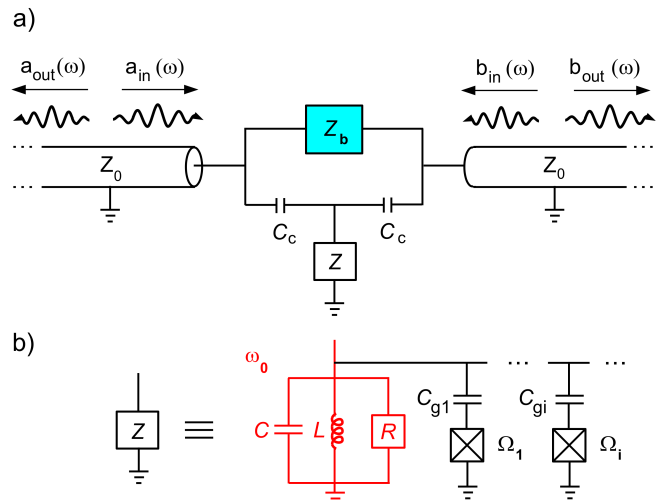


FIG. 1: (a) Incoming and outgoing microwave fields propagate in two semi-infinite transmission lines with characteristic impedance Z_0 . They are connected via capacitors C_c to a microwave cavity modeled by element Z . The transmission lines are also connected directly to each other through background impedance Z_b . (b) The coplanar microwave cavity is described by an LCR resonator [21]. Superconducting transmon artificial atoms [22] (crossed boxes), with energy-level differences between the ground and the first excited states $\hbar\Omega_i$, are embedded in the cavity. They couple to the resonator through coupling capacitors C_{gi} .

impedances, is presented and compared to our model in Appendix A.

A. Microwave radiation in transmission lines

1. Propagation states

Fano physics appear in microwave propagation across a cavity with parallel background. Microwave radiation in the left TL is described by a traveling-field solution for the magnetic flux [14, 23–25]

$$\hat{\Phi}(x < 0, t) = \sqrt{\frac{\hbar Z_0}{2\omega_0}} [\hat{a}_{\text{in}}(t - x/c) + \hat{a}_{\text{out}}(t + x/c) + \text{H.c.}] . \quad (1)$$

We associate the position $x = 0$ as the cavity boundary and the space is semi-infinite, $-\infty < x < 0$. The capacitance C' and inductance L' per unit length define the characteristic impedance $Z_0 = \sqrt{L'/C'}$ and the speed of light $c = 1/\sqrt{L'C'}$. We work in the narrow-bandwidth approximation [23] and therefore the cavity resonance frequency ω_0 (defined below) appears in the equation. The operator $\hat{a}_{\text{in}}^{(\dagger)}(t)$ annihilates (creates) an incoming photon. These operators satisfy the commuta-

tion relations

$$[\hat{a}_{\text{in}}(t), \hat{a}_{\text{in}}^\dagger(t')] = \delta(t - t'). \quad (2)$$

The same relation needs to be valid also for the corresponding outgoing-field photon operators $\hat{a}_{\text{out}}(t)$ (which we can solve as a function input fields) in order the theory to be consistent [26].

We also define photon operators of specific frequencies

$$\hat{a}_{\text{in/out}}(\omega) = \frac{1}{\sqrt{2\pi}} \int_{-\infty}^{\infty} dt e^{i\omega t} \hat{a}_{\text{in/out}}(t). \quad (3)$$

We have then

$$\hat{a}_{\text{in/out}}(t) = \frac{1}{\sqrt{2\pi}} \int_{-\infty}^{\infty} d\omega e^{-i\omega t} \hat{a}_{\text{in/out}}(\omega). \quad (4)$$

The commutation relations of these fixed-frequency operators have the form

$$[\hat{a}_{\text{in}}(\omega), \hat{a}_{\text{in}}^\dagger(\omega')] = \delta(\omega - \omega'). \quad (5)$$

A similar definition is made also for the operators describing fields on the right of the cavity, \hat{b}_{in} and \hat{b}_{out} .

2. Considered microwave reflection and transmission functions

The main properties we study in the following are the microwave reflection, $s_{11}(\omega)$, and microwave transmission, $s_{12}(\omega)$, amplitudes. They are defined through the output states when having a coherent input from one side (and no input from the other side). By assuming a coherent input of frequency ω from the left, we define

$$s_{11}(\omega) = \frac{\langle \hat{a}_{\text{out}}(\omega) \rangle}{\langle \hat{a}_{\text{in}}(\omega) \rangle} \quad (6)$$

$$s_{12}(\omega) = \frac{\langle \hat{b}_{\text{out}}(\omega) \rangle}{\langle \hat{a}_{\text{in}}(\omega) \rangle}. \quad (7)$$

These relations are solved by using microwave boundary conditions and equations of motion for the cavity and artificial atoms, as described below.

B. Cavity boundary conditions I: Model without a background

1. Transmission line connected to a cavity

We continue building our model by considering first the simplest situation: When there are no transmons embedded in the cavity, no parallel transmission ($Z_b = \infty$), and no intrinsic dissipation ($R = \infty$). We treat the photonic state inside the cavity as a single-mode system, described

by the Hamiltonian

$$\hat{H}_0 = \hbar\omega_0 \hat{a}^\dagger \hat{a}. \quad (8)$$

Here the operator $\hat{a}^{(\dagger)}$ is the cavity photon annihilation (creation) operator satisfying $[\hat{a}, \hat{a}^\dagger] = 1$. The TL-coupling normalized resonance frequency is here

$$\omega_0 = \frac{1}{\sqrt{L(C + 2C_c)}}. \quad (9)$$

Here L (C) is the inductance (capacitance) of the cavity and C_c the coupling capacitance between the cavity and a transmission line, see Fig. 1.

An interaction between the semi-infinite TLs and the cavity is described by boundary conditions at the two sides of the cavity [14]. On the left-hand side we write

$$\hat{a}_{\text{out}}(t) = \sqrt{\gamma} \hat{a}(t) - \hat{a}_{\text{in}}(t). \quad (10)$$

The operators are time dependent since the condition is given in the Heisenberg picture. Similarly for the right-hand side,

$$\hat{b}_{\text{out}}(t) = \sqrt{\gamma} \hat{a}(t) - \hat{b}_{\text{in}}(t). \quad (11)$$

The decay rate is identical in the two directions and has the form

$$\gamma = \left(\frac{C_c}{C + 2C_c} \right)^2 \frac{Z_0}{Z_{LC}} \omega_0, \quad (12)$$

where the characteristic impedance of the resonator is $Z_{LC} = \sqrt{L/(C + 2C_c)}$. This treatment is valid for high quality factor cavities, $Q = \omega_0/\gamma \gg 1$, and usual cavity-transmon couplings, $g \ll \omega_0$ (well below the ultra-strong coupling regime).

The cavity field operator also satisfies [14]

$$\hat{a}(t) = \frac{i}{\hbar} \left[\hat{H}_0, \hat{a}(t) \right] - \gamma \hat{a}(t) + \sqrt{\gamma} \left[\hat{a}_{\text{in}}(t) + \hat{b}_{\text{in}}(t) \right]. \quad (13)$$

This Heisenberg equation of motion is found to be also more generally valid, with proper redefinition of Hamiltonian \hat{H}_0 , accounting for the presence of artificial atoms, and even in the presence of reactive and dissipative parallel coupling.

2. Interaction with two-level systems

It is straightforward to account for the presence of artificial atoms in the above treatment. Including artificial atoms as two-level systems in the rotating-wave approximation ($g_i \ll \omega_0$) [14] we obtain the Tavis-Cummings Hamiltonian

$$\hat{H}_0 = \hbar\omega_0 \hat{a}^\dagger \hat{a} + \hbar \sum_{i=1}^n \frac{\Omega_i}{2} \hat{\sigma}_z^i + \sum_{i=1}^n \hbar g_i (\hat{a}^\dagger \hat{\sigma}_-^i + \hat{a} \hat{\sigma}_+^i). \quad (14)$$

Here $\hat{\sigma}_{+(-)}^i$ is the spin raising (lowering) operator of two-level system i . Boundary conditions (10-11) and Heisenberg equation of motion (13) keep their form.

In this article we work mainly in the dispersive regime, where $g_i \ll |\Delta|$ and $\Delta = \Omega_i - \omega_0$. This coupling regime is commonly used for readout of superconducting qubits [11]. An effective Hamiltonian for a single-atom system is here [5]

$$\hat{H}_0 = \hbar \left(\omega_0 + \frac{g^2}{\Delta} \hat{\sigma}_z \right) \hat{a}^\dagger \hat{a} + \frac{\hbar}{2} \left(\Omega_0 + \frac{g^2}{\Delta} \right) \hat{\sigma}_z. \quad (15)$$

Corrections to this Hamiltonian are higher orders in $g/\Delta \ll 1$. The effective resonance frequency of the cavity then depends on the state of the two-level system and can have values $\omega_0 \pm g^2/\Delta$. This type of Hamiltonian can be used to describe a driven cavity, if the neglected energy-level anharmonicity is small compared to the energy-level broadening [16]. For low photon-number distributions the relevant condition is $g^2/|\Delta| \times (g/\Delta)^2 \ll \gamma$, which is assumed to be true when considering a dispersive regime in this article.

Generalization to multiple two-level systems in the dispersive regime is

$$\hat{H}_0 = \hbar \left(\omega_0 + \sum_{i=1}^n \frac{g_i^2}{\Delta_i} \hat{\sigma}_z \right) \hat{a}^\dagger \hat{a} + \frac{\hbar}{2} \sum_{i=1}^n \left(\Omega_0 + \frac{g_i^2}{\Delta_i} \right) \hat{\sigma}_z. \quad (16)$$

Here $\Delta_i = \Omega_i - \omega_0$ and we assume a negligible interaction between the two-level systems via the cavity.

3. Interaction with transmons

In our experiment, the cavity interacts with 8 transmon artificial atoms. Here, the artificial-atom resonance properties are well described by parallel $L_i C_i$ circuits and the coupling by capacitor C_{gi} , see Fig. 1(b). The explicit couplings are here [22]

$$\hbar g_i = \frac{\hbar}{2} \sqrt{\omega_0 \Omega_i} \frac{C_{gi}}{\sqrt{C C_i}}. \quad (17)$$

We assume here small coupling capacitors, $C_{gi}, C_c \ll C, C_i$. The two-level splittings are in a good approximation $\Omega_i = 1/\sqrt{L_i(C_i + C_{gi})}$ and the bare cavity frequency $\omega_0 = 1/\sqrt{L(C + 2C_c + \sum_i C_{gi})}$.

For transmons, the dispersive shifts are not as in Eqs. (15-16), since higher energy levels need to be accounted for [22]. This is because the second energy-level splitting, $\hbar\Omega - E_C$, where $E_C = e^2/2(C_i + C_{gi}) \ll \hbar\Omega$, is close to the first splitting $\hbar\Omega$. A correction to the dispersive-shift operator of a single transmon is accounted for by a replacement [22]

$$\frac{g^2}{\Delta} \hat{\sigma}_z \hat{a}^\dagger \hat{a} \leftarrow \left(\frac{g^2}{\Delta} - \frac{g^2}{\Delta - E_C/\hbar} \right) \hat{\sigma}_z \hat{a}^\dagger \hat{a}. \quad (18)$$

In the limit $E_C = 0$, there is no anharmonicity and the shift vanishes. In the hypothetical limit $E_C = \infty$ the shift would agree with the two-level system, Eq. (15). Also here a simple additivity of the dispersive shifts in the case of multi-transmon environment is valid. The dispersive shifts of a multi-transmon system as well as of higher excited states of single transmons have been studied detailed experimentally in Refs. [27–29].

C. Cavity boundary conditions II: Including a background

We now extend the above model to also include non-dissipative parallel transmission. The boundary conditions of Eqs. (10-11) can be shown to generalize to (Appendix B)

$$\hat{a}_{\text{out}}(t) = \sqrt{\gamma} \hat{a}(t) - \frac{1}{1 + 2i\epsilon} \hat{a}_{\text{in}}(t) - \frac{2i\epsilon}{1 + 2i\epsilon} \hat{b}_{\text{in}}(t) \quad (19)$$

$$\hat{b}_{\text{out}}(t) = \sqrt{\gamma} \hat{a}(t) - \frac{1}{1 + 2i\epsilon} \hat{b}_{\text{in}}(t) - \frac{2i\epsilon}{1 + 2i\epsilon} \hat{a}_{\text{in}}(t). \quad (20)$$

Here we have introduced a parameter describing the reactive response of a parallel inductance L_b

$$\epsilon = \frac{Z_0}{\omega_0 L_b} = \frac{Z_0}{|Z_b(\omega_0)|}. \quad (21)$$

We consider explicitly the case of a parallel inductor, whereas the result for a parallel capacitor is obtained by a sign change $\epsilon \rightarrow -\epsilon$ (Appendix C). Dissipation will be included later in Sec. II E. The limit $\epsilon \rightarrow 0$ then gives the previous input-output relations for two-sided cavity, Eqs. (10-11).

The Heisenberg equation of motion for the cavity field, Eq. (13), stays the same, irrespective of the values of γ and ϵ . This result means that previous models for driven cavities [15, 16, 27, 30] or dispersive quantum-state measurement [11, 22] can be generalized to the presence of background transmission by accounting for the modified boundary conditions (19-20) when evaluating properties of the outgoing fields from the (unchanged) solution for the cavity field.

D. Solution for a linear cavity

In the case of a linear cavity, we can solve the out-fields as a function of input directly by Fourier transformation. This solution is valid also for a cavity-transmon system in the dispersive limit when no transmon transitions occur, or when transitions are slow and can be accounted for by

statistical averaging. In such cases we have

$$\begin{pmatrix} \hat{a}_{\text{out}}(\omega) \\ \hat{b}_{\text{out}}(\omega) \end{pmatrix} = \frac{1}{(1+2i\epsilon)(1-2if)} \quad (22)$$

$$\times \begin{pmatrix} 4\epsilon f - 1 & -2i(\epsilon + f) \\ -2i(\epsilon + f) & 4\epsilon f - 1 \end{pmatrix} \begin{pmatrix} \hat{a}_{\text{in}}(\omega) \\ \hat{b}_{\text{in}}(\omega) \end{pmatrix},$$

where

$$f(\omega) = \frac{\gamma}{2(\omega_0 - \omega)}. \quad (23)$$

The possible dispersive shift of the cavity frequency is now incorporated in ω_0 .

The scattering amplitude can be shown to be here

$$s_{12} = \frac{2\epsilon}{i-2\epsilon} + \frac{\gamma}{\gamma + i(\omega_0 - \omega)} \quad (24)$$

$$= \frac{\gamma + 2\epsilon(\omega_0 - \omega)}{(1+2i\epsilon)[\gamma + i(\omega_0 - \omega)]}.$$

The special cases $\epsilon = 0$ or $\gamma = 0$ give the transmission amplitudes when the parallel transmission does not contribute or the cavity does not contribute, correspondingly. The reflection amplitude has the form

$$s_{11} = -\frac{1}{1+2i\epsilon} + \frac{\gamma}{\gamma + i(\omega_0 - \omega)} \quad (25)$$

$$= \frac{2\epsilon\gamma + \omega - \omega_0}{(-i+2\epsilon)[\gamma + i(\omega_0 - \omega)]}.$$

For a non-dissipative system the transmission and reflection powers sum to 1,

$$|s_{11}|^2 + |s_{12}|^2 = 1. \quad (26)$$

Here, the solution also satisfies the commutation relations

$$[\hat{a}_{\text{out}}(t), \hat{a}_{\text{out}}^\dagger(t')] = \delta(t-t') \quad (27)$$

$$[\hat{b}_{\text{out}}(t), \hat{b}_{\text{out}}^\dagger(t')] = \delta(t-t'), \quad (28)$$

which is obtained only by assuming that this is true for the input fields, Eq. (2), demonstrating consistency of the theory.

E. Including dissipation and fluctuations

Now we discuss how to account for the effect of dissipation and finite temperature. We include these as average effects by tracing out environmental degrees of freedom of the decoherence sources. Note that when decoherence is included in this way, the (above derived) energy conservation and the commutation relations are not necessarily anymore valid.

1. Dissipative background and dissipative cavity

We obtain that a finite resistivity of the background can be introduced phenomenologically by adding a negative imaginary part to parameter ϵ , i.e., replacing

$$\epsilon \leftarrow \epsilon - i\epsilon_d \quad (29)$$

in the generalization of Sec. II C. The relation to the resistivity of impedance $Z_b(\omega)$ is discussed in Appendix A. Our approach is generally valid for small dissipative parts, $\epsilon_d \ll 1$. Note that variables ϵ and ϵ_d are dimensionless.

It is well known that intrinsic dissipation of the cavity field can be introduced in an exactly the same way, by adding an imaginary part to the resonance frequency, i.e., replacing

$$\omega_0 \leftarrow \omega_0 - i\omega_d. \quad (30)$$

This corresponds in the parallel *LCR*-circuit of Fig. 1 to [24] $\omega_d = 1/2RC = \omega_0/2Q$, where in the second form we have defined a quality factor $Q = \omega_0 RC$. The equivalent energy decay rate is then

$$\frac{1}{RC} = 2\omega_d. \quad (31)$$

This approach is valid for $\omega_d \ll \omega_0$. Later, in Sec. III, we find that this simple trick can also describe a dephasing effect of the cavity in the dispersive regime, due to heating of the environment.

2. Finite temperature and master-equation formulation

The effect of heating is included here using a master-equation formulation. Thermal radiation plays a role only in the case of a non-linear cavity, since otherwise for average fields, such as in Eqs. (6-7), thermal fluctuations average out. This is since here (in the steady state) thermal fluctuations only define the width of the Gaussian probability distribution of the quadratures, around the classical means [14]. Similarly, thermal radiation emitted by the background directly in the output is not expected to contribute to average quadratures.

We can simulate a driven cavity-transmon system by using a Lindblad master equation [14]

$$\dot{\hat{\rho}} = \frac{i}{\hbar}[\hat{\rho}, \hat{H}] + \mathcal{L}_a[\hat{\rho}] + \mathcal{L}_b[\hat{\rho}] + \mathcal{L}_{\text{decoh}}[\hat{\rho}] + \sum_{i=1}^n \mathcal{L}_{qi}[\hat{\rho}]. \quad (32)$$

Here $\hat{\rho}$ is the reduced density matrix of the resonator and two-level systems and operators \mathcal{L} are defined below. We use a Hamiltonian

$$\hat{H} = \hat{H}_0 + \hat{H}_d, \quad (33)$$

where an incoming coherent field from side *a* is accounted

for by a term

$$\hat{H}_a = i\hbar\sqrt{\gamma}A(t)\hat{a}^\dagger + \text{H.c.}, \quad (34)$$

which can be derived by assuming

$$\langle \hat{a}_{\text{in}}(t) \rangle = A(t), \quad (35)$$

and $\langle \hat{b}_{\text{in}}(t) \rangle = 0$, and that in the far past the cavity and transmission-line states are independent [14].

The corresponding total Hamiltonian of a driven cavity coupled to single two-level system in the dispersive limit can be written in the form

$$\begin{aligned} \hat{H} = & \hbar \left(\omega_0 - \omega + \frac{g^2}{\Delta} \hat{\sigma}_z \right) \hat{a}^\dagger \hat{a} + \frac{\hbar}{2} \left(\Omega_0 + \frac{g^2}{\Delta} \right) \hat{\sigma}_z \\ & + \frac{\alpha}{2} (\hat{a} + \hat{a}^\dagger). \end{aligned} \quad (36)$$

Here we have shifted to a rotating frame with respect to drive frequency ω and assume that $\alpha = 2i\hbar\sqrt{\gamma}A(t)e^{i\omega t}$ is a constant real number.

As previously, we assume $g \ll \omega_0, \Omega_i$ and that possible differences between decay rates related to different shifted values of the cavity frequency can be neglected. The Lindblad super-operator \mathcal{L}_a then describes cavity transitions due to interaction with the left TL,

$$\mathcal{L}_a[\hat{\rho}] = \frac{\gamma^-}{2} (2\hat{a}\hat{\rho}\hat{a}^\dagger - \hat{a}^\dagger\hat{a}\hat{\rho} - \hat{\rho}\hat{a}^\dagger\hat{a}) \quad (37)$$

$$+ \frac{\gamma^+}{2} (2\hat{a}^\dagger\hat{\rho}\hat{a} - \hat{a}\hat{a}^\dagger\hat{\rho} - \hat{\rho}\hat{a}\hat{a}^\dagger). \quad (38)$$

This form follows from the Heisenberg equations of motion. The decay rate to the left TL satisfies in thermal equilibrium

$$\gamma^- = \gamma \left[1 + \frac{1}{\exp\left(\frac{\hbar\omega_0}{k_B T}\right) - 1} \right], \quad (39)$$

and correspondingly for the thermal excitation rate

$$\gamma^+ = \gamma \left[\frac{1}{\exp\left(\frac{\hbar\omega_0}{k_B T}\right) - 1} \right]. \quad (40)$$

We have then $\gamma^- = \gamma^-(T=0) + \gamma^+$. Similarly for the interaction with right TL described by super-operator \mathcal{L}_b .

The intrinsic cavity decoherence we consider has two contributions,

$$\mathcal{L}_{\text{decoh}} = \mathcal{L}_{\text{loss}} + \mathcal{L}_{\text{deph}}, \quad (41)$$

where the intrinsic cavity loss operator $\mathcal{L}_{\text{loss}}$ has an analogous form as \mathcal{L}_a . The intrinsic cavity 'pure dephasing' operator $\mathcal{L}_{\text{deph}}$ is in the considered single-photon (low

drive power) limit

$$\mathcal{L}_{\text{deph}}[\hat{\rho}] = \frac{\omega_{\text{deph}}}{2} (\hat{\sigma}_a \hat{\rho} \hat{\sigma}_a - \hat{\rho}). \quad (42)$$

Here we have defined $\hat{\sigma}_a = \hat{a}^\dagger \hat{a} - 1/2$ in analogy to σ_z operator of a two-level system.

Finally, intrinsic dissipation and fluctuations of two-level systems can be added by Lindblad super-operators

$$\mathcal{L}_{qi}[\hat{\rho}] = \frac{\gamma_{qi}^-}{2} (2\hat{\sigma}_-^i \hat{\rho} \hat{\sigma}_+^i - \hat{\sigma}_+^i \hat{\sigma}_-^i \hat{\rho} - \hat{\rho} \hat{\sigma}_+^i \hat{\sigma}_-^i) \quad (43)$$

$$+ \frac{\gamma_{qi}^+}{2} (2\hat{\sigma}_+^i \hat{\rho} \hat{\sigma}_-^i - \hat{\sigma}_-^i \hat{\sigma}_+^i \hat{\rho} - \hat{\rho} \hat{\sigma}_-^i \hat{\sigma}_+^i), \quad (44)$$

where γ_{qi}^\pm is the corresponding transition rate of two-level system i . These rates are affected by the electromagnetic environment as seen by the transmons [20]. The effect of pure dephasing of the two-level systems can be included similarly as the effect of cavity dephasing.

The average output fields, $\langle \hat{a}_{\text{out}}(t) \rangle$ and $\langle \hat{b}_{\text{out}}(t) \rangle$, and the possible interference effect between the cavity and the background, can then be solved by first determining $\langle \hat{a}(t) \rangle$ from a steady-state solution for the master equation (32). After this one applies Eqs. (19-20) to account for the interference between the background and cavity transmission. Here one also inserts the assumed average, $\langle \hat{a}_{\text{in}}(t) \rangle = A(t)$. The form of the interference in different situations is analyzed in Sec. III.

III. FANO RESONANCES IN THEORY

In this section, we investigate the line shape of microwave transmission across the two-sided cavity with background in different conditions. We start in Sec. III A from a short introduction to the form of the conventional Fano-resonance function and in Sec. III B identify it in the case of a linear cavity with no internal or background dissipation. In Sec. III C, we study the influence of dissipation and pure dephasing in the case of a linear cavity. We find that intrinsic cavity loss and pure dephasing of the cavity affect the transmission amplitude s_{12} in the very same way. In Sec. III D, we study Fano-type resonances when the cavity is dispersively connected to two-level systems subjected to heating-induced incoherent transitions.

A. Conventional Fano function

In a Fano resonance [1–3], the spectral response of a resonant system is asymmetric around the resonance frequency due to an interference effect between two scattering amplitudes: Scattering through a background with a constant (or wide) state density and scattering through a discrete (or narrow) energy-level. The conventional form of the Fano interference is characterized by only single

variable: Fano parameter q . Here, the total scattering amplitude $|s|$, or spectral density $|s|^2$, are of the form (neglecting normalization factors)

$$|s| \propto \frac{|q + \eta|}{\sqrt{1 + \eta^2}}, \quad |s|^2 \propto \frac{(q + \eta)^2}{1 + \eta^2}, \quad (45)$$

where η is a broadening-normalized drive frequency with respect to the resonance frequency, $\eta = (\omega_0 - \omega)/(\Gamma/2)$, with Γ being a parameter describing the resonant-state broadening. Two central limits of this function are $q \rightarrow \infty$, giving a Lorentzian shaped *peak*, and $q = 0$, giving a Lorentzian shaped *dip*. This description then catches resonant enhancement as well as resonant suppression as two limits of one function.

B. Decoherence-free linear oscillator

We consider first Fano resonances in the case of dissipation-free linear cavity. This analysis covers also Jaynes- or Tavis-Cummings oscillators in the dispersive limit when two-level-system transitions do not occur, or when the transitions are slow and statistical averaging is possible. Here one can use the analytical solutions of Eqs. (24-25). We get

$$|s_{12}|^2 = \frac{1}{1 + q^2} \frac{(q + \eta)^2}{1 + \eta^2}. \quad (46)$$

Here we have identified

$$q = \frac{1}{2\epsilon} \quad (47)$$

$$\eta = \frac{\omega_0 - \omega}{\gamma}. \quad (48)$$

From Eq. (21) we obtain that for $|Z_b(\omega_0)| \rightarrow \infty$ we have the limit $q \rightarrow \infty$ and transmission probability $|s_{12}|^2$ approaches a Lorentzian peak. For any finite parallel coupling (finite q) interference occurs. It is perfectly destructive when $q = -\eta$, meaning

$$\omega = \omega_0 + \frac{\gamma}{2\epsilon}. \quad (49)$$

The response near the resonance frequency can also be a dip, $q = 0$, when $|Z_b(\omega_0)| \rightarrow 0$. Such form then needs a very strong parallel transmission.

For all systems we consider after this we have $\epsilon \ll 1$, which for a non-dissipative and coherent system leads to a tilted peak, $q \gg 1$.

C. Linear oscillator with decoherence and dissipative background

We consider now including dissipation in the cavity when having a weak parallel transmission, $\epsilon \ll 1$. A finite

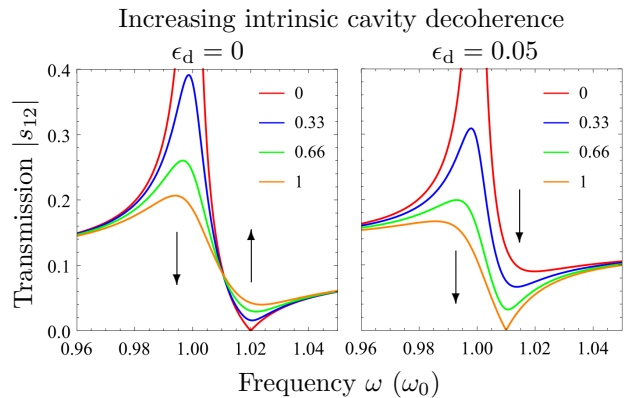


FIG. 2: The effect of intrinsic cavity decoherence (loss or dephasing) to transmission $|s_{12}(\omega)|$ in the presence of weak background transmission $\epsilon = 0.05$. We increase the decoherence rate ω_d as indicated by the plot legends in units of $10^{-2}\omega_0$, the curve changing as pointed by the arrows. Without dissipation in the background ($\epsilon_d = 0$), increase of cavity decoherence lowers the maximum and increases the minimum of $|s_{12}(\omega)|$. With a dissipative background ($\epsilon_d = 0.05$) both minimum and maximum decrease with increasing cavity decoherence in the considered range $\omega_d \in [0, 0.01]\omega_0$. For higher ω_d the minimum starts to rise (not plotted). We consider a linear cavity with resonance frequency ω_0 and coupling to each transmission line $\gamma = 2 \times 10^{-3}\omega_0$.

intrinsic quality factor of the cavity can be accounted for by adding an imaginary part $\omega_0 \leftarrow \omega_0 - i\omega_d$. The solution of Eq. (24) is valid also here. Furthermore, we find that intrinsic cavity loss and pure dephasing of the cavity affect the average transmission amplitude s_{12} in the same way. The effect is identical when

$$\omega_d = \omega_{\text{deph}}. \quad (50)$$

Note that the equivalent internal energy decay rate is $1/RC = 2\omega_d$, Sec. III E 1.

Transmission $|s_{12}(\omega)|$ for several values of decoherence rate ω_d is shown in Fig. 2 ($\epsilon_d = 0$). We find that the intrinsic decoherence reduces transmission and 'straightens' the interference structure. The reflection dip also gets less deep (not plotted).

Consider then adding small dissipation also in the (weak) parallel transmission. A finite resistivity in the parallel channel can be accounted for by a replacement $\epsilon \leftarrow \epsilon - i\epsilon_d$. We first note that without a reactive part in the parallel channel (finite ϵ), we never get an asymmetric resonance curve (tilt). Again, resistivity in the parallel channel reduces transmission on resonance, but the two dissipative effects do not simply sum up as an effective increased cavity dissipation rate. Instead, if we assume a fixed background dissipation and increase the cavity dissipation (or dephasing), an interesting effect appears: The minimum value of $|s_{12}|$ decreases with increasing cavity decoherence and reaches zero, see Fig. 2 ($\epsilon_d = 0.05$). For larger cavity decoherence rates the minimum increases again (plotted in Fig. 7). The reflection

$|s_{11}|$, Eq. (25), is also here always a dip.

From Eq. (24) we obtain analytically that the minimum transmission is exactly zero when

$$\omega_d = \frac{\gamma}{2} \frac{\epsilon_d}{\epsilon^2 + \epsilon_d^2}. \quad (51)$$

This zero transmission occurs for

$$\omega = \omega_0 + \frac{\gamma}{2} \frac{\epsilon}{\epsilon^2 + \epsilon_d^2}. \quad (52)$$

D. Jaynes-Cummings oscillator

As another example we consider a cavity with no internal losses ($\omega_d = 0$) but which has a dispersive coupling to a two-level system exhibiting incoherent transitions between the two states. In the model we use Hamiltonian (15) and solve the steady-state expectation value $\langle \hat{a} \rangle$ and transmission s_{12} for weak drive powers, as described in Sec. III E.

The resulting transmission $|s_{12}(\omega)|$ as a function of identical hopping rates $\gamma_q^+ = \gamma_q^-$ (high-temperature limit) without background is plotted in Fig. 3 (left panel). Two interesting limits appear. Firstly, if the excitation and decay rates are small compared to the system dynamics (rate γ), the solution for the transmission is a statistical average over two results, corresponding to the two frequencies of the dispersively-shifted cavity. Secondly, when the excitation and decay rates dominate the dispersive shift, $2g^2/\Delta$, motional averaging appears [31], where switching is so fast that only the average value of the cavity frequency is observed.

When a weak parallel transmission with dissipation is included, Fig. 3 (right panel), the low-hopping rate peaks are changed to skewed Fano-type peaks. When the hopping rates are increased, the skewed peaks evolve into dips. A change in the interference structure is possible since here transmission through the (nonlinear) cavity changes, but is constant across the (linear) background. A motionally-averaged common dip emerges in the limit of high hopping rates. Finally, a skewed Fano-type peak is recovered in the limit of very high hopping rates. We note that a similar line-shape transformation can also occur without the presence of dispersive-shift hopping, but, for example, when increasing the drive power [17] due to a cavity transmission blockade at moderate drive powers [16].

Two important effects for the analysis of our experiment are present in the simulation in Fig. 3. These are peak transformation due to (i) reduced resonant-state population and (ii) fast incoherent-transition induced dephasing, which occur at weak and moderate hopping rates, correspondingly.

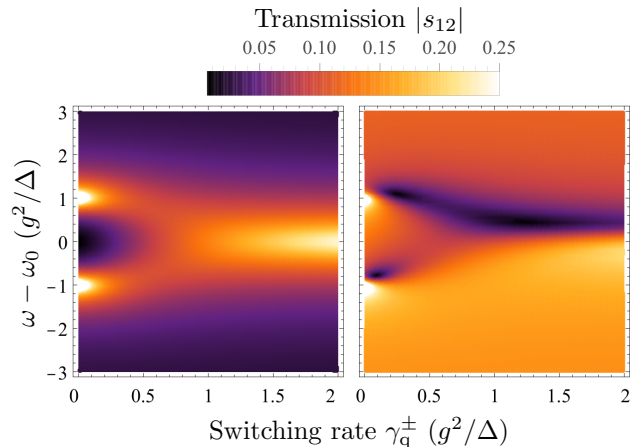


FIG. 3: Transmission across a Jaynes-Cummings oscillator with a dispersive shift that switches incoherently between two values separated by $2g^2/\Delta$. We consider a situation without ($\epsilon = \epsilon_d = 0$, left panel) and with ($\epsilon = \epsilon_d = 0.05$, right panel) a background transmission. The switching rate γ_q^\pm is the same for both directions and the dispersive shift is much larger than the cavity linewidth, $g^2/\Delta = 13\gamma$, and $\gamma = 10^{-3}\omega_0$. Without a background transmission (left panel) and with weak switching rates, $\gamma_q^\pm < \gamma$, we observe a statistical average of transmission for two equally-populated cavity-frequency states. When increasing the switching rate, the two transmission peaks merge into a motional-averaged single resonance peak [31]. In the presence of a weak dissipative background transmission (right panel), the two Fano-type peaks evolve to two dips (when $\gamma_q^\pm \gtrsim \gamma$) and finally from a single motional-averaged dip to a single tilted peak.

1. Reduced resonant-state population

We study first more detailed the effect of reduced population of the resonant state. We consider the population p to be an arbitrary number below 1. Such a reduced population can occur due to excitations of the artificial atoms to states with dispersive shifts far away from the broadened resonance. We consider here a regime where the switching is much slower than the cavity decay to TLs, $\gamma^{+/-} \ll \gamma$, so that its effect is to just change state populations, not to induce a dephasing effect discussed in Sec. III D 2.

Applying Eq. (24) by assuming that the transmission through the cavity in the non-resonant state is zero, meaning (background) transmission $2(\epsilon - i\epsilon_d)/(i - 2\epsilon + 2i\epsilon_d)$ with probability $1 - p$, we get

$$s_{12} = \frac{2\eta + p - 2\epsilon_d(1 - p) - 2i[\epsilon(1 - p) + \eta]}{1 + i\eta}. \quad (53)$$

Here again $\eta = (\omega_0 - \omega)/\gamma$. The effect of reducing probability p is visualized in Fig. 4. For the dissipation-free background, Fig. 4 ($\epsilon_d = 0$), the interference structure 'straightens', but for the dissipative background, Fig. 4 ($\epsilon_d = 0.05$), the transmission becomes increasingly skewed and touches zero. For even lower populations it

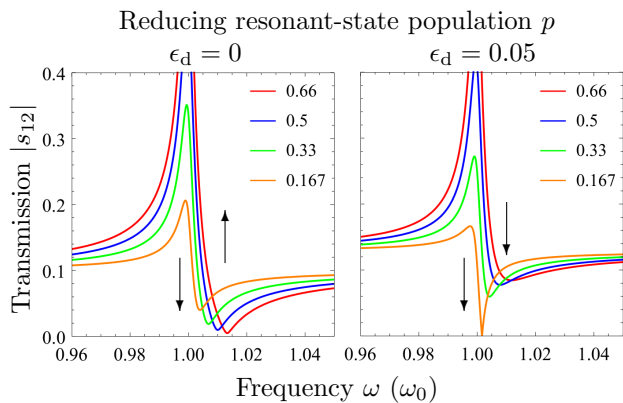


FIG. 4: Transmission across Jaynes-Cummings oscillator with resonant-state population p and weak background transmission $\epsilon = 0.05$. We decrease p as indicated by the plot legends, the curve changing as pointed by the arrows. In the case of dissipation-free background ($\epsilon_d = 0$) the reduction in population decreases the maximum and increases the minimum transmission. In the case of dissipative background ($\epsilon_d = 0.05$) the reduction in population decreases the maximum and the minimum transmission in the shown range of p . We consider a resonance frequency ω_0 and coupling to each transmission line $\gamma = 2 \times 10^{-3}\omega_0$.

approaches a straight line (plotted in Fig. 8). The curve touches zero with population

$$p = 1 - \frac{\epsilon_d}{\epsilon_d + 2\epsilon_d^2 + 2\epsilon^2}. \quad (54)$$

The frequency where this occurs is

$$\omega = \omega_0 + \frac{\epsilon\gamma}{\epsilon_d + 2\epsilon_d^2 + 2\epsilon^2}. \quad (55)$$

In additional simulations we obtain that the effect of increasing temperature in a photon-blockade limit [15], i.e., when only one photon per time is allowed to enter the cavity (at low drive powers), is very similar to the effect of reducing p in the above analysis. This is since here thermal cavity photons play the same role as reduced resonant-state population: They block transmission across the cavity. In Sec. IV, we present an experimental observation of this effect.

2. Cavity dephasing

Fast two-level system switching can also induce dephasing of the signal propagating through the cavity. A clean example of this effect (not mixed with the reduced population effect, Sec. III D 1) is when we have a high asymmetry between excitation and decay rates, $\gamma_q^+ \ll \gamma_q^-$, leading to that $p \approx 1$. Here, the two-level system is mostly in its ground state with stochastic short-time visits in its excited state. This creates a similar effect to s_{12} as cavity dissipation. These two effects are

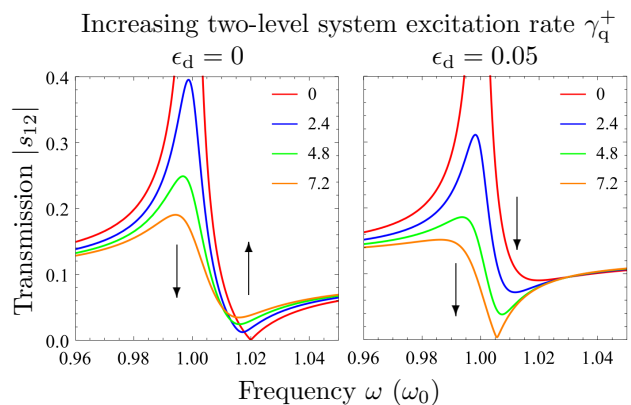


FIG. 5: Transmission across Jaynes-Cummings oscillator when increasing two-level system excitation rate γ_q^+ with weak background transmission $\epsilon = 0.05$. We consider a large dispersive shift, $g^2/\Delta = -40\gamma$, and fast two-level system decay, $\gamma_q^-(T=0) = 5\gamma$, and $\gamma_q^+(T=0) = 0$. The transition rates γ_q^- and γ_q^+ are (both) increased as indicated by the plot legends in units of $10^{-3}\gamma$, the curve changing as pointed by the arrows. In the case of dissipation-free background ($\epsilon_d = 0$), the heating decreases the maximum and increases the minimum transmission. In the case of dissipative background ($\epsilon_d = 0.05$), the heating decreases the maximum and minimum transmission in the considered range of γ_q^+ . The resonance frequency ω_0 accounts for the dispersive shift of the ground state and coupling to each transmission line is $\gamma = 2 \times 10^{-3}\omega_0$.

indeed equivalent in the limit of fast decay and large dispersive shift.

The change of the transmission curve with increasing the excitation rate γ_q^+ is plotted in Fig. 5. We simultaneously increase the relaxation rate with the same amount, as implied by thermal equilibrium statistics, Eqs. (39-40). The total dispersive shift is assumed to be much larger than the cavity broadening, $|2g^2/\Delta| \gg \gamma$, and we consider a weak drive power. We find that the effect is very similar to having a linear cavity with intrinsic decoherence rate (see also Fig. 2 in comparison to Fig. 5)

$$\omega_d \approx \gamma_q^+. \quad (56)$$

The effects are the same in the limit of fast decay $\gamma_q^-(T=0) \gg \gamma$ and large dispersive shift $g^2/\Delta \gg \gamma_q^-(T=0)$.

The similarity to internal decay can be understood as that in this limit a single jump of the two-level system is enough to dephase the system, and that for superpositions of photon numbers the effect of dephasing and decay is qualitatively the same.

Taking use of the analogy between increased cavity decoherence and incoherent-transitions induced dephasing we find that approximately when

$$\gamma_q^+ \approx \frac{\gamma}{2} \frac{\epsilon_d}{\epsilon^2 + \epsilon_d^2}, \quad (57)$$

the transmission $|s_{12}(\omega)|$ touches zero, following from Eq. (51).

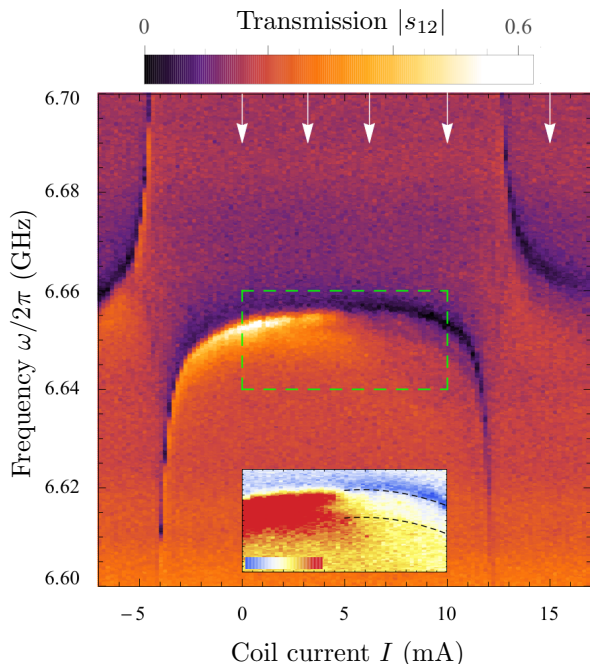


FIG. 6: Measured microwave transmission $|s_{12}|$ through a coplanar cavity coupled to 8 transmons as a function of coil current I , used to tune one transmon, and drive frequency ω . The resonance position is periodic as a function of the current (transmon inductance), whereas the line shape transforms from a peak to a dip when current $|I|$ is increased. Transmission curves at pointed current bias points are plotted in Fig. 7. (Inset) Transmission inside the dashed rectangle. For $I \gtrsim 5$ mA, the resonance inversion emerges together with a peak splitting and transmission plateau (between the dashed lines), indicating finite populations of excited states of transmons. The colorbar changes from 0 to 0.3.

In the presence of multiple two-level systems, for relaxation rates much higher than the excitation rates, $\gamma_{qi}^- \gg \gamma_{qi}^+$, and with strong dispersive shifts, the transmission $|s_{12}(\omega)|$ is expected to touch zero approximately when

$$\sum_i \gamma_{qi}^+ \approx \frac{\gamma}{2} \frac{\epsilon_d}{\epsilon^2 + \epsilon_d^2}. \quad (58)$$

It should be noted that in both effects studied in this section, i.e., in reduced resonant-state population and in cavity dephasing, the resonance inversion is of statistical nature and observable only after long-time averaging. Quantitatively: Even though $s_{12}(\omega) \propto \langle \hat{b}_{\text{out}}(\omega) \rangle$ is zero for certain ω , the photon flux density, proportional to $\langle \hat{b}_{\text{out}}^\dagger(\omega) \hat{b}_{\text{out}}(\omega) \rangle$, is not necessarily zero.

IV. EXPERIMENT AND COMPARISON TO THEORY

In our experiment, 8 transmon artificial atoms are embedded in a driven coplanar microwave resonator [17].

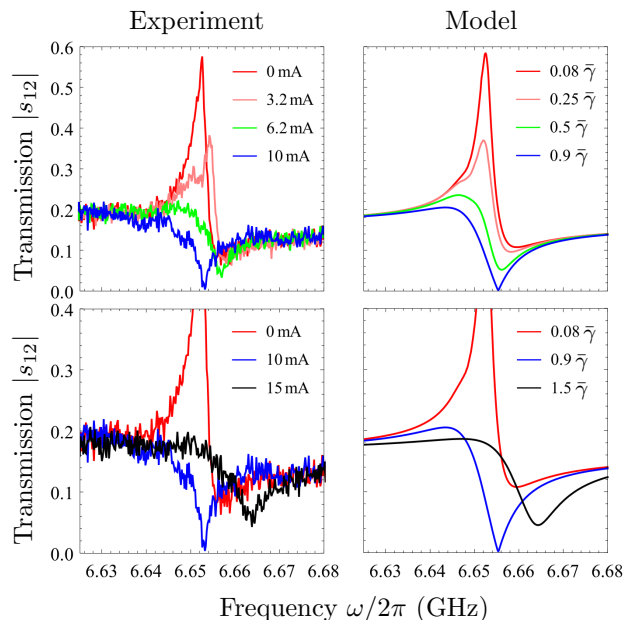


FIG. 7: (left) Experimental data of Fig. 6 for indicated values of coil current I , showing a transition from a peak to a dip when current is increased. (right) A theoretical change of the line shape as given by a model of a heated Tavis-Cummings oscillator and a weakly-coupled microwave background. The model accounts for one transmon as a two-level system with dispersive coupling $2g^2/\Delta = 2\pi \times 5$ MHz and other transmons via a dephasing rate ω_{deph} given in units of $\bar{\gamma} = 3.85\gamma$. The microwave background is described by $\epsilon = \epsilon_d = 0.065$. A thermal excitation rate of the two-level system is assumed to be $\gamma_q^+ = \omega_{\text{deph}}/4$ and zero temperature decay rate $\gamma_q^-(T=0) = \gamma = 2\pi \times 1$ MHz.

The energy levels of the transmons are individually tunable by applying magnetic fluxes across Josephson inductors realized in a SQUID geometry. The magnetic fluxes are created by DC bias currents through 8 nearby coils. The energy levels of this multi-atom environment affect the cavity resonance frequency, which is probed by measuring the microwave transmission s_{12} at base temperature $T \approx 20$ mK.

An example of measured weak-drive-power transmission s_{12} is shown in Fig. 6. Here we probe the system in the neighborhood of the dispersively-shifted cavity $n = 1$ mode. This mode has pure frequency $\omega_0/2\pi = 6.674$ GHz. The data is normalized according to transmission at high powers. We sweep single coil current I to tune one transmon. All other coil currents are zero. We observe an avoided energy-level crossing between the cavity and the tuned transmon. The observed resonance-frequency variation is periodic as a function of current I , as expected from SQUID-flux periodicity. An additional random offset flux threads the SQUID loops leading to an offset from the symmetry-point $I = 0$. The transmission however reduces with increasing $|I|$, not following the flux-periodicity, with a line shape changing from a peak to a dip.

The experimental data is compared to our theoretical model in Fig. 7 for several values of bias current I . At these bias points the cavity-transmon coupling is dispersive. Our simplified model accounts for one transmon as a two-level system with dispersive coupling $2g^2/\Delta$ and other (heated) transmons via a cavity dephasing rate ω_{deph} . The dephasing rate for each curve is indicated in 'inversion' units $\bar{\gamma} = \gamma\epsilon_d/2(\epsilon^2 + \epsilon_d^2) = 3.85\gamma$, see Eq. (51). A thermal excitation (and induced emission) rate of the two-level system is assumed to be $\gamma_q^+ = \omega_{\text{deph}}/4$. The theoretical curve for $\gamma_q^+ = 1.5\bar{\gamma}$ is shifted rightwards by 9.5 MHz to account for the changed absolute shift of the resonator due to the energy-level crossing, not included by the model.

In the model we use the hypothesis that DC current causes heating of the bias lead(s) and of the cavity-atom system. Heating, or a presence of stochastic fluctuations, is supported by two central observations. Firstly, the line-shape transformation matches to theory of increasing decoherence, Sec. III C. Secondly, the reduction in transmission comes together with features that indicate a presence of multiple dispersive shifts, i.e., finite populations of excited states of transmons. For example, in the data of Fig. 6, a sensitized plot (inset) reveals a peak splitting and a transmission plateau of width ~ 5 MHz, emerging just below the (ground-state) resonance frequency. This feature is recognizable also in Fig. 7. In the experiment, we have average cavity-transmon couplings $g_i/2\pi \approx 120$ MHz and anharmonicities $E_C \approx 410$ MHz [17], which implies that this feature originates from a transmon (or several of them) at distance $|\Delta| = |\Omega - \omega_0| \sim 2\pi \times 2$ GHz, Eq. (18). This feature is reproduced qualitatively by the inclusion of the two-level system in the model of Fig. 7.

In our model we include a reactive and dissipative microwave background described by $\epsilon = \epsilon_d = 0.065$. These parameters becomes fixed by the strength of the off-resonance background transmission as well as by the way the resonance transforms during the inversion. When expressed using a background impedance $Z_b = 1/i\omega C_b + R_b$ (Appendix A) this environment corresponds to a capacitor $C_b = 47$ fF and resistor $R_b = 370 \Omega$. Such capacitive coupling can occur through the multiple DC flux bias lines beside the cavity, supported by microwave simulations, which give a similar capacitive coupling across these leads. However, the coupling from the input conductor to the bias leads does not occur through a direct coupling between the cavity and nearby conducting strips, for which we simulate a value $\lesssim 3$ fF. It is most likely mediated via sample box walls. The resistance $R_b = 370 \Omega$ is close to the impedance of the free space (377Ω), suggesting emission loss to free space. Background transmission as well as cavity-transmission reduction (when increasing control current) were not present in an additional experiment that included only single transmon in the cavity.

The contribution from multiple transmons and possibly also from their higher excited states makes an estima-

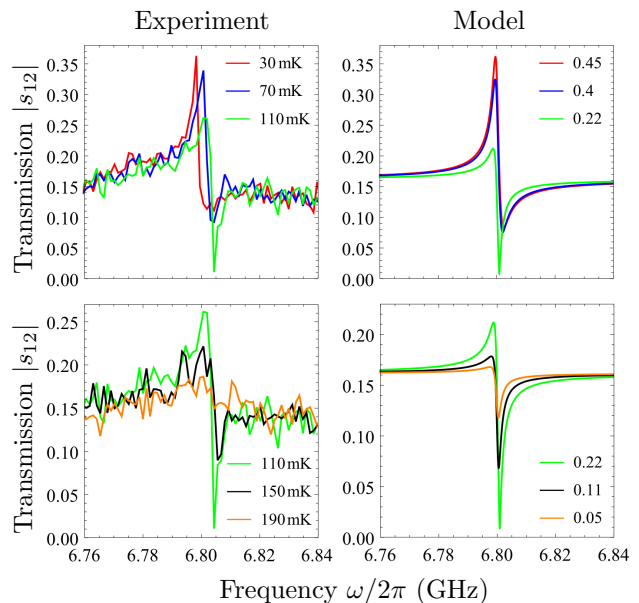


FIG. 8: (left) Measured transmission $|s_{12}|$ at different base temperatures. We are tuned close to a resonance between the cavity and a transmon, where one thermal photon in the cavity blocks the resonant transmission. (right) A theoretical change of the line shape based on the model of reduced resonant-state population, with indicated probabilities p , Sec. III D 1. The microwave background is described by $\epsilon = \epsilon_d = 0.065$.

tion of the system temperature using the model difficult. In the fit of Fig. 7, the peak has changed to a dip approximately when $\gamma_q^+(T) \sim \gamma_q^-(T=0)$. For a two-level system with $\Omega/2\pi \sim 6$ GHz this needs $T \sim 0.4$ K. Additional experiments on base-temperature dependence however imply that for large coil currents $T \sim 0.2$ K. (The base temperature itself was experimentally found to depend on the coil currents only weakly.) Such difference to the model can appear, on one hand, since the theory includes only one transmon as a two-level system and switchings of others via an effective dephasing rate, and on the other hand, since higher excited states and possible other decoherence sources of the transmon(s) have been neglected. In such simplified model the used excitation and dephasing rates should be then considered as effective (fitting) parameters. This is to compare with a full set of parameters describing 8 transmons, their coupling to the cavity, and their coupling to an environment.

The resonance inversion is observed also by increasing the base temperature of the experiment. In Fig. 8, we show the effect of base temperature (in another cool-down) when being tuned close to the avoided crossing between the cavity and one transmon. One tuning coil is biased at $I = 1.1$ mA, whereas all other coils at zero. The main difference to the previously-studied dispersive regime is that here the presence of one or more thermal photons in the cavity blocks the resonant transmission. Thermal excitations of the cavity are then expected to have a similar effect as reduced resonant-state popula-

tion, Sec. III D 1. The observed change of the line shape follows rather well the transformation as given by this model, Fig. 8.

V. CONCLUSIONS AND DISCUSSION

In this work we have investigated Fano resonances in microwave transmission through a cavity coupled to multiple artificial atoms and in the presence of a microwave background. The background was effectively formed by the artificial-atom control circuitry. State-of-the-art (and beyond) microwave quantum-information devices commonly include multiple qubits and their control lines in a finite sized chip and a sample box, where Fano resonances may easily occur. We have then studied in detail how the line shapes of the system energy levels connect to decoherence and nonlinearities in this system, helping to more easily understand possibly complex spectroscopic data of such devices.

An important theoretical result is that the background does not necessarily affect the equation of motion of the cavity and artificial atoms. Instead, it can be included to theoretical results obtained from the well-known Jaynes- and Tavis-Cummings models afterwards by applying linear boundary conditions. Its effect can then also be subtracted out ("undone") straightforwardly from measurement results. This property remains to be valid also for time-dependent fields (measurement pulses), higher drive

powers, and beyond the two-level-system and dispersive approximations.

It should also be noted that all dephasing mechanisms of superconducting microwave resonators due to coupling to spurious two-level systems [32–35] are not yet fully understood. The results obtained here for the emergence and behavior of Fano-type resonances also apply to studies of such systems generally. On the other hand, systems as described here can also be used as quantum simulators of the involved physical phenomena.

Acknowledgments

This work was supported by the European Research Council (ERC) under the Grant Agreement 648011, Deutsche Forschungsgemeinschaft (DFG) within Project No. WE4359/7-1, the Initiative and Networking Fund of the Helmholtz Association, the China Scholarship Council (CSC), and Studienstiftung des deutschen Volkes. We also acknowledge support provided by the Initiative and Networking Fund of the Helmholtz Association, within the Helmholtz Future Project Scalable solid state quantum computing. This work was also partially supported by the Ministry of Education and Science of the Russian Federation in the framework of the Program to Increase Competitiveness of the NUST MISIS, contract no. K2-2017-081.

-
- [1] U. Fano, Phys. Rev. **124**, 1866 (1961), URL <https://link.aps.org/doi/10.1103/PhysRev.124.1866>.
 - [2] M. F. Limonov, M. V. Rybin, A. N. Poddubny, and Y. S. Kivshar, Nature Photonics **11**, 543 (2017), URL <https://doi.org/10.1038/nphoton.2017.142>.
 - [3] A. E. Miroshnichenko, S. Flach, and Y. S. Kivshar, Rev. Mod. Phys. **82**, 2257 (2010), URL <https://doi.org/10.1103/RevModPhys.82.2257>.
 - [4] B. Lv, R. Li, J. Fu, Q. Wu, K. Zhang, W. Chen, Z. Wang, and R. Ma, Sci. Rep. **6**, 31884 (2016), URL <https://dx.doi.org/10.1038/srep31884>.
 - [5] A. Blais, R.-S. Huang, A. Wallraff, S. M. Girvin, and R. J. Schoelkopf, Phys. Rev. A **69**, 062320 (2004), URL <https://doi.org/10.1103/PhysRevA.69.062320>.
 - [6] M. H. Devoret and R. J. Schoelkopf, Science **339**, 1169 (2013), URL <https://doi.org/10.1126/science.1231930>.
 - [7] X. Gu, A. F. Kockum, A. Miranowicz, Y. X. Liu, and F. Nori, Phys. Rep. **718-719**, 1 (2017), URL <https://doi.org/10.1016/j.physrep.2017.10.002>.
 - [8] S. Krinner, S. Storz, P. Kurpiers, P. Magnard, J. Heinsoo, R. Keller, J. Luetolf, C. Eichler, and A. Wallraff, *Engineering cryogenic setups for 100-qubit scale superconducting circuit systems* (2018), URL <https://arxiv.org/abs/1806.07862>.
 - [9] R.-P. Riwar, A. Hosseinkhani, L. D. Burkhardt, Y. Y. Gao, R. J. Schoelkopf, L. I. Glazman, and G. Catelani, Phys. Rev. B **94**, 104516 (2016), URL <https://doi.org/10.1103/PhysRevB.94.104516>.
 - [10] D. Bothner, D. Wiedmaier, B. Ferdinand, R. Kleiner, and D. Koelle, Phys. Rev. Applied **8**, 034025 (2017), URL <https://doi.org/10.1103/PhysRevApplied.8.034025>.
 - [11] A. Wallraff, D. I. Schuster, A. Blais, L. Frunzio, J. Majer, M. H. Devoret, S. M. Girvin, and R. J. Schoelkopf, Phys. Rev. Lett. **95**, 060501 (2005), URL <https://doi.org/10.1103/PhysRevLett.95.060501>.
 - [12] M. Tavis and F. W. Cummings, Phys. Rev. **170**, 379 (1968), URL <https://doi.org/10.1103/PhysRev.170.379>.
 - [13] J. M. Fink, M. Göppl, M. Baur, R. Bianchetti, P. J. Leek, A. Blais, and A. Wallraff, Nature **454**, 315 (2008), URL <http://dx.doi.org/10.1038/nature07112>.
 - [14] D. F. Walls and G. Milburn, *Quantum Optics* (Springer, Berlin, 2008).
 - [15] L. S. Bishop, J. M. Chow, J. Koch, A. A. Houck, M. H. Devoret, E. Thuneberg, S. M. Girvin, and R. J. Schoelkopf, Nature Phys. **5**, 105 (2009), URL <https://doi.org/10.1038/nphys1154>.
 - [16] L. S. Bishop, E. Ginossar, and S. M. Girvin, Phys. Rev. Lett. **105**, 100505 (2010), URL <https://link.aps.org/doi/10.1103/PhysRevLett.105.100505>.
 - [17] P. Yang, J. D. Brehm, J. Leppäkangas, L. Guo, M. Marthaler, I. Boventer, A. V. Ustinov, and M. Weides, *In preparation*.

- [18] A. Schneider, J. Braumüller, L. Guo, P. Stehle, H. Rotzinger, M. Marthaler, A. V. Ustinov, and M. Weides, *Phys. Rev. A* **97**, 062334 (2018), URL <https://doi.org/10.1103/PhysRevA.97.062334>.
- [19] J. Braumüller, M. Marthaler, A. Schneider, A. Stehli, H. Rotzinger, M. Weides, and A. V. Ustinov, *Nat. Commun.* **8**, 779 (2017), URL <https://doi.org/10.1038/s41467-017-00894-w>.
- [20] J. Leppäkangas, J. Braumüller, M. Hauck, J.-M. Reiner, I. Schwenk, S. Zanker, L. Fritz, A. V. Ustinov, M. Weides, and M. Marthaler, *Phys. Rev. A* **97**, 052321 (2018), URL <https://doi.org/10.1103/PhysRevA.97.052321>.
- [21] M. Göppl, A. Fragner, M. Baur, R. Bianchetti, S. Filipp, J. M. Fink, P. J. Leek, G. Puebla, L. Steffen, and A. Wallraff, *Journal of Applied Physics* **104**, 113904 (2008), URL <http://dx.doi.org/10.1063/1.3010859>.
- [22] J. Koch, T. M. Yu, J. Gambetta, A. A. Houck, D. I. Schuster, J. Majer, A. Blais, M. H. Devoret, S. M. Girvin, and R. J. Schoelkopf, *Phys. Rev. A* **76**, 042319 (2007), URL <http://link.aps.org/doi/10.1103/PhysRevA.76.042319>.
- [23] R. Loudon, *The Quantum Theory of Light* (Oxford University Press, New York, 2010).
- [24] D. M. Pozar, *Microwave Engineering*, 2nd ed. (Wiley, New York, 1998).
- [25] J. Leppäkangas, M. Marthaler, D. Hazra, S. Jebari, R. Albert, F. Blanchet, G. Johansson, and M. Hofheinz, *Phys. Rev. A* **97**, 013855 (2018), URL <https://doi.org/10.1103/PhysRevA.97.013855>.
- [26] M. E. Peskin and D. V. Schroeder, *An Introduction To Quantum Field Theory* (Addison-Wesley Publishing Company, 1995).
- [27] M. D. Reed, L. DiCarlo, B. R. Johnson, L. Sun, D. I. Schuster, L. Frunzio, and R. J. Schoelkopf, *Phys. Rev. Lett.* **105**, 173601 (2010), URL <https://doi.org/10.1103/PhysRevLett.105.173601>.
- [28] M. J. Peterer, S. J. Bader, X. Jin, F. Yan, A. Kamal, T. J. Gudmundsen, P. J. Leek, T. P. Orlando, W. D. Oliver, and S. Gustavsson, *Phys. Rev. Lett.* **114**, 010501 (2015), URL <https://doi.org/10.1103/PhysRevLett.114.010501>.
- [29] J. Braumüller, J. Cramer, S. Schlör, H. Rotzinger, L. Radtke, A. Lukashenko, P. Yang, S. T. Skacel, S. Probst, M. Marthaler, et al., *Phys. Rev. B* **91**, 054523 (2015), URL <https://doi.org/10.1103/PhysRevB.91.054523>.
- [30] J. M. Fink, A. Dombi, A. Vukics, A. Wallraff, and P. Domokos, *Phys. Rev. X* **7**, 011012 (2017), URL <https://doi.org/10.1103/PhysRevX.7.011012>.
- [31] J. Li, M. P. Silveri, K. S. Kumar, J.-M. Pirkkalainen, A. Vepsäläinen, W. C. Chien, J. Tuorila, M. A. Siljanpää, P. J. Hakonen, E. V. Thuneberg, et al., *Nat. Commun.* **4**, 1420 (2013), URL <http://dx.doi.org/10.1038/ncomms2383>.
- [32] J. Gao, J. Zmuidzinas, B. A. Mazin, H. G. LeDuc, and P. K. Day, *Appl. Phys. Lett.* **90**, 102507 (2007), URL <http://dx.doi.org/10.1063/1.2711770>.
- [33] M. R. Vissers, M. P. Weides, J. S. Kline, M. Sandberg, and D. P. Pappas, *Appl. Phys. Lett.* **101**, 022601 (2012), URL <https://doi.org/10.1063/1.4730389>.
- [34] J. Burnett, L. Faoro, I. Wisby, V. L. Gurtovoi, A. V. Chernykh, G. M. Mikhailov, V. A. Tulin, R. Shaikhaidarov, V. Antonov, P. J. Meeson, et al., *Nat. Commun.* **5**, 4119 (2014), URL <http://dx.doi.org/10.1038/ncomms5119>.
- [35] S. E. de Graaf, L. Faoro, J. Burnett, A. A. Adamyan, A. Y. Tzalenchuk, S. E. Kubatkin, T. Lindström, and A. V. Danilov, *Nat. Commun.* **9**, 1143 (2018), URL <http://dx.doi.org/10.1038/s41467-018-03577-2>.

Appendix A: Linear scattering model

In this appendix, we apply a classical circuit model to study microwave transmission and reflection in our system. This model assumes that the whole system can be described as a set of lumped circuit elements. The model accounts for superconducting artificial atoms by treating them as classical resonators.

In this approach, we derive scattering properties by applying Kirchhoff rules at the cavity boundaries. For this, we first identify the total voltage and total current due to forward (in) and backward (out) propagating fields at the two sides of the cavity. On the left-hand side these are [24]

$$V^L = V_{\text{in}}^L + V_{\text{out}}^L \quad (\text{A1})$$

$$I^L = \frac{V_{\text{in}}^L}{Z_0} - \frac{V_{\text{out}}^L}{Z_0} \quad (\text{A2})$$

and on the right-hand side

$$V^R = V_{\text{in}}^R + V_{\text{out}}^R \quad (\text{A3})$$

$$I^R = -\frac{V_{\text{in}}^R}{Z_0} + \frac{V_{\text{out}}^R}{Z_0}. \quad (\text{A4})$$

These variables are Fourier components of the total propagating field, e.g., $V^L = V^L(\omega)$. The reflection s_{11} and the transmission s_{12} amplitudes are here

$$s_{11}^* = \frac{V_{\text{out}}^L}{V_{\text{in}}^L} \quad (\text{A5})$$

$$s_{12}^* = \frac{V_{\text{out}}^R}{V_{\text{in}}^L}. \quad (\text{A6})$$

We assume here $V_{\text{in}}^R = 0$. The complex conjugation is needed here in comparison to Eqs. (6-7) since the impedance treatment assumes implicitly a time dependence $\sim V(\omega)e^{i\omega t}$, which is opposite to the time dependence of annihilation operators $\sim \hat{a}(\omega)e^{-i\omega t}$.

We first consider the case of parallel impedance ($C_c = 0$). This gives two boundary conditions, which state current conservation and voltage drop across the impedance $Z_b(\omega)$,

$$\frac{V_{\text{in}}^L}{Z_0} - \frac{V_{\text{out}}^L}{Z_0} = -\frac{V_{\text{in}}^R}{Z_0} + \frac{V_{\text{out}}^R}{Z_0} \quad (\text{A7})$$

$$Z_b \left(\frac{V_{\text{in}}^L}{Z_0} - \frac{V_{\text{out}}^L}{Z_0} \right) = V_{\text{in}}^L + V_{\text{out}}^L - (V_{\text{in}}^R + V_{\text{out}}^R). \quad (\text{A8})$$

Using $V_{\text{in}}^{\text{R}} = 0$ the solution is

$$s_{11}^* = \frac{1}{1 + \frac{2Z_0}{Z_b}} \quad (\text{A9})$$

$$s_{12}^* = \frac{\frac{2Z_0}{Z_b}}{1 + \frac{2Z_0}{Z_b}}. \quad (\text{A10})$$

We can now study more detailed the effect of dissipation in the parallel channel. In the main text this was done by introducing the imaginary part, $\epsilon_{\text{tot}} = \epsilon - i\epsilon_{\text{d}}$. In the impedance approach the equivalent parameter is $i\epsilon_{\text{tot}} = Z_0/Z_b^*(\omega) = Z_0 Z_b / |Z_b^*(\omega)|^2$. Dissipation is included, for example, by changing the impedance from $Z_b(\omega) = i\omega L_p \omega$ to $Z_b(\omega) = i\omega L_b \omega + R_b$, with a series resistance $R_b > 0$. This approach also shows that a dissi-

pative part renormalizes the reactive term ϵ . This is studied further below. We note that in a direct comparison of Eqs. (A9-A10) to s_{11} and s_{12} given in the main text, Eqs. (24-25), an overall minus-sign difference appears due to different definition of scattering-state phases, for more details see Appendix B.

Similarly, we can construct boundary conditions for arbitrary cavity couplings $Z_{c1} = 1/i\omega C_{c1}$ and $Z_{c2} = 1/i\omega C_{c2}$. Here we allow for different coupling capacitance of the cavity to the left-hand side (C_{c1}) and the right-hand side (C_{c2}) TLs. We then consider Kirchhoff equations for the input and output fields as well for the voltage on the island between capacitances $C_{c1/2}$, which we mark now V . The resulting equations have the form

$$\begin{pmatrix} \frac{1}{Z_0} + \frac{1}{Z_{c1}(\omega)} + \frac{1}{Z_p(\omega)} & & & \\ & -\frac{1}{Z_{c1}(\omega)} & & \\ & & \frac{1}{Z(\omega)} + \frac{1}{Z_{c1}(\omega)} + \frac{1}{Z_{c2}(\omega)} & \\ & & & -\frac{1}{Z_0} - \frac{1}{Z_{c2}(\omega)} - \frac{1}{Z_p(\omega)} \end{pmatrix} \begin{pmatrix} V_{\text{out}}^{\text{L}} \\ V \\ V_{\text{out}}^{\text{R}} \end{pmatrix} = \begin{pmatrix} \frac{1}{Z_0} - \frac{1}{Z_{c1}(\omega)} - \frac{1}{Z_p(\omega)} \\ \frac{1}{Z_{c1}(\omega)} \\ -\frac{1}{Z_p(\omega)} \end{pmatrix} V_{\text{in}}^{\text{L}},$$

The answer for the output fields and for the island voltage as a function of the input V_{in}^{L} can then be found easily by a matrix inversion. For the considered symmetric coupling, $C_{c1} = C_{c2} = C_c$, the analytical solution is

$$s_{11}^* = \frac{2Z_0 [Z_c^2 + Z(2Z_c + Z_p)]}{(2Z + Z_0 + Z_c) [Z_0(2Z_c + Z_p) + Z_c Z_p]} \quad (\text{A11})$$

$$s_{12}^* = \frac{Z_c Z_p (2Z + Z_c) - Z_0^2 (2Z_c + Z_p)}{(2Z + Z_0 + Z_c) [Z_0(2Z_c + Z_p) + Z_c Z_p]}. \quad (\text{A12})$$

A comparison between the single-mode treatment of the main text and the impedance approach considered here is shown in Fig. 9. We consider dissipationless background transmission. Here, the impedance model is exact whereas the single-cavity-mode model used in the main text is an approximation. We find that if $C_c \ll C$, the single-cavity-mode model works well for all strengths of parallel transmission, i.e., for all values of ϵ .

A comparison in the case of dissipative background is shown in Fig. 10. We determine $\epsilon_{\text{tot}} = \epsilon - i\epsilon_{\text{d}}$ from identification $i\epsilon_{\text{tot}} = Z_0/Z_b^*(\omega) = Z_0 Z_b / |Z_b^*(\omega)|^2$ by using $Z_b(\omega) = i\omega L_p \omega + R_b$ and insert this parameter into the single-mode model. We find again that for $C_c \ll C$ the exact linear solution and the approximative single-cavity-mode model are practically the same. However, we need to emphasize that for $\epsilon_{\text{d}} \sim 1$ the solution for a non-linear system is not necessary reliable, since damping is not included in the cavity drive. Therefore, unless the model can be shown to be valid in specific cases for all ϵ_{d} , a restriction to weak dissipation, $\epsilon_{\text{d}} \ll 1$, should be considered.

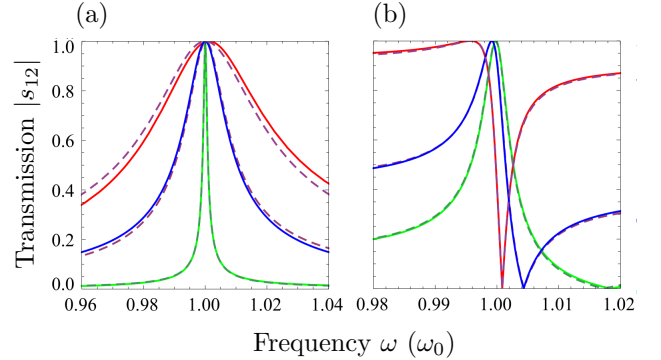


FIG. 9: Microwave transmission amplitude $|s_{12}|$ across a linear two-sided cavity. We do comparison between the single-mode treatment (solid lines) and impedance approach (dashed lines). The cavity is described by an LC oscillator. (a) Transmission without the presence of background transmission with $C_c/C = 0.05, 0.2, 0.4$. In the single-mode approximation this corresponds to $\gamma = (0.5, 8, 32) \times 10^{-3}\omega_0$. The single-mode treatment is here a good approximation and becomes exact in the limit $C_c/C \rightarrow 0$. (b) Transmission for $C_c/C = 0.1$ with increasing dissipationless background transmission corresponding to $\epsilon = 0.05, 0.2, 1.0$. Here, the single-mode treatment is a good approximation for all strengths of the background transmission.

Appendix B: Deriving boundary conditions and Heisenberg equations of motion

The boundary conditions and Heisenberg equations of motion can be derived by starting from a Lagrangian approach for an open transmission line interacting with a

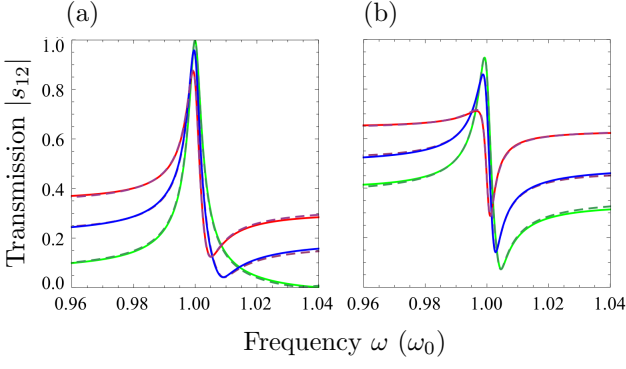


FIG. 10: Microwave transmission amplitude $|s_{12}|$ across a linear two-sided cavity for different parallel impedances. We do comparison between the single-mode treatment (solid lines) and impedance approach (dashed lines). (a) Transmission for $C_c/C = 0.1$ with reducing inductance with fixed resistivity. The equivalent ϵ -parameters are $\epsilon = 0.025, 0.054, 0.10, 0.13, 0.18$ and dissipative part $\epsilon_d = 0.0015, 0.006, 0.023, 0.04, 0.08$. (b) Transmission for $C_c/C = 0.1$ with reducing inductance further with fixed resistivity. The equivalent ϵ -parameters are $\epsilon = 0.21, 0.25, 0.32, 0.42, 0.50$ and dissipative part $\epsilon_d = 0.046, 0.070, 0.12, 0.23, 0.55$.

cavity. Here, we discretize the transmission line to elements of length δx with capacitance to ground $\delta x C'$ and inductance $\delta x L'$ in between. We apply this approach to the case of free cavity (no transmons), whereas generalization to the case of cavity embedding multiple transmons is straightforward.

In this approach, the total Hamiltonian of the system can be derived to be

$$H_{\text{tot}} = H_{\text{R}} + H_{\text{L}} + H_{\text{res}} + H_{\text{int}}. \quad (\text{B1})$$

The Hamiltonian that describes the right-hand open transmission line is

$$H_{\text{R}} = \sum_{r=2}^{\infty} \frac{Q_r^2}{2\delta x C'} + \sum_{r \geq 2}^{\infty} \frac{(\Phi_r - \Phi_{r-1})^2}{2L'\delta x} \quad (\text{B2})$$

$$+ \frac{QQ_1}{C} + \frac{Q_1^2}{2C_s}.$$

Indices $r \in [1, \infty]$ refer to nodes of the discretized transmission line, value $r = 1$ corresponds to the node next to the cavity. Variables Φ_r and Q_r correspond to a magnetic flux and charge at node r and an effective series capacitance is defined as $1/C_s = 1/C_c + 1/C$. The flux (charge) variable of the resonator is Φ (Q). Similarly for the left-hand side Hamiltonian,

$$H_{\text{L}} = \sum_{l=-\infty}^{-2} \frac{Q_l^2}{2\delta x C'} + \sum_{l \leq -1} \frac{(\Phi_l - \Phi_{l-1})^2}{2L'\delta x} \quad (\text{B3})$$

$$+ \frac{QQ_{-1}}{C} + \frac{Q_{-1}^2}{2C_s}.$$

A Hamiltonian that describes the in-line resonator is

$$H_{\text{res}} = \frac{Q^2}{2C} + \frac{\Phi^2}{2L}. \quad (\text{B4})$$

The inductance L and capacitance C are defined in Fig. 1(b). Finally, the direct interaction between the two transmission lines (background) is described by

$$H_{\text{int}} = \frac{(\hat{\Phi}_1 - \hat{\Phi}_{-1})^2}{2L_b} + \frac{Q_{-1}Q_1}{C}, \quad (\text{B5})$$

where L_b is the assumed inductive coupling through the background. Also a direct-coupling-type term through the resonator appears.

The Heisenberg equations of motion for the transmission lines in the limit $\delta x \rightarrow 0$ result in a wave equation whose solution can be written as in Eq. (1).

The Heisenberg equations at the node $r = 1$ are

$$\hat{\Phi}_1(t) = \frac{\hat{Q}}{C} + \frac{\hat{Q}_{-1}}{C} + \frac{\hat{Q}_1}{C_s} \quad (\text{B6})$$

$$\hat{Q}_1(t) = \frac{1}{L'} \frac{\partial \hat{\Phi}(x=0^+, t)}{\partial x} + \frac{\hat{\Phi}_{-1} - \hat{\Phi}_1}{L_b}. \quad (\text{B7})$$

Similarly for the left-hand side ($l = -1$)

$$\hat{\Phi}_{-1}(t) = \frac{\hat{Q}}{C} + \frac{\hat{Q}_1}{C} + \frac{\hat{Q}_{-1}}{C_s} \quad (\text{B8})$$

$$\hat{Q}_{-1}(t) = -\frac{1}{L'} \frac{\partial \hat{\Phi}(x=0^-, t)}{\partial x} + \frac{\hat{\Phi}_1 - \hat{\Phi}_{-1}}{L_b}. \quad (\text{B9})$$

Eq. (B7) is satisfied by

$$\hat{Q}_1(t) = \sqrt{\frac{\hbar}{2\omega_0 Z_0}} [-\hat{b}_{\text{in}}(t) + \hat{b}_{\text{out}}(t)] \quad (\text{B10})$$

$$+ \frac{i}{\omega_0 L_p} \sqrt{\frac{\hbar Z_0}{2\omega_0}} [\hat{a}_{\text{in}}(t) + \hat{a}_{\text{out}}(t)]$$

$$- \frac{i}{\omega_0 L_p} \sqrt{\frac{\hbar Z_0}{2\omega_0}} [\hat{b}_{\text{in}}(t) + \hat{b}_{\text{out}}(t)] + \text{H.c.}$$

Similarly

$$\hat{Q}_{-1}(t) = \sqrt{\frac{\hbar}{2\omega_0 Z_0}} [-\hat{a}_{\text{in}}(t) + \hat{a}_{\text{out}}(t)] \quad (\text{B11})$$

$$+ \frac{i}{\omega_0 L_p} \sqrt{\frac{\hbar Z_0}{2\omega_0}} [\hat{b}_{\text{in}}(t) + \hat{b}_{\text{out}}(t)]$$

$$- \frac{i}{\omega_0 L_p} \sqrt{\frac{\hbar Z_0}{2\omega_0}} [\hat{a}_{\text{in}}(t) + \hat{a}_{\text{out}}(t)] + \text{H.c.}$$

Our approach to find an approximative solution for this problem is the following. We first assume that $\omega_c \equiv 1/C_s Z_0 \gg \omega_0$ and can thereby neglect the time derivatives in Eqs. (B6) and (B8). Within this approximation we can directly establish boundary conditions

between the cavity and TL fields to be used later. This approximation can be shown to correspond to neglecting terms $\ll \gamma$ in final equation of motion for the cavity. This simplification leads to boundary conditions

$$\hat{Q}_{-1} = -\hat{Q} \frac{C_c}{C + 2C_c} \quad (\text{B12})$$

$$\hat{Q}_1 = -\hat{Q} \frac{C_c}{C + 2C_c}. \quad (\text{B13})$$

Using Eqs. (B10-B12) and inserting $\hat{Q} = i\sqrt{\frac{\hbar}{2Z_{LC}}} [\hat{a}^\dagger(t) - \hat{a}(t)]$ we get

$$\alpha \hat{a}(t) = -\hat{a}_{\text{in}}(t) + \hat{a}_{\text{out}}(t) + \epsilon [\hat{a}_{\text{in}}(t) + \hat{a}_{\text{out}}(t)] + \epsilon^* [\hat{b}_{\text{in}}(t) + \hat{b}_{\text{out}}(t)] \quad (\text{B14})$$

$$\epsilon = i \frac{Z_0}{\omega_0 L_p} \quad (\text{B15})$$

$$\alpha = -i \frac{C_c}{C + 2C_c} \sqrt{\frac{Z_0}{Z_{LC}}} \sqrt{\omega_0}. \quad (\text{B16})$$

Here we choose $Z_{LC} = \sqrt{L/(C + 2C_c)}$ (and $\omega_0 = 1/\sqrt{L(C + 2C_c)}$) since this choice removes mixing of \hat{a} and \hat{a}^\dagger in the following cavity equations of motion, i.e., diagonalizes an equivalent cavity Hamiltonian. We have also implicitly assumed that there is no mixing between annihilation and creation operators between the system and the environment, following from a rotating-wave approximation.

Analogously we establish a solution using Eq. (B13),

$$\alpha \hat{a}(t) = -\hat{b}_{\text{in}}(t) + \hat{b}_{\text{out}}(t) + \epsilon [\hat{b}_{\text{in}}(t) + \hat{b}_{\text{out}}(t)] + \epsilon^* [\hat{a}_{\text{in}}(t) + \hat{a}_{\text{out}}(t)]. \quad (\text{B17})$$

The boundary conditions given in the main text follow a convention used in Ref. [14] and correspond to redefinition of the phase of the incoming field operator as $\hat{a}_{\text{in}} \leftarrow -i\hat{a}_{\text{in}}$ and the outgoing-field operator as $\hat{a}_{\text{out}} \leftarrow i\hat{a}_{\text{out}}$. Similarly $\hat{b}_{\text{in}} \leftarrow -i\hat{b}_{\text{in}}$ and $\hat{b}_{\text{out}} \leftarrow i\hat{b}_{\text{out}}$. It should be noted that in comparison to the impedance approach, we have now effectively changed the signs of out field amplitudes, changing signs of functions s_{11} and s_{12} . The previously-derived boundary conditions are in this notation

$$\alpha \hat{a}(t) = \hat{a}_{\text{in}}(t) + \hat{a}_{\text{out}}(t) + i\epsilon [-\hat{a}_{\text{in}}(t) + \hat{a}_{\text{out}}(t)] - i\epsilon [-\hat{b}_{\text{in}}(t) + \hat{b}_{\text{out}}(t)] \quad (\text{B18})$$

$$\alpha \hat{a}(t) = \hat{b}_{\text{in}}(t) + \hat{b}_{\text{out}}(t) + i\epsilon [-\hat{b}_{\text{in}}(t) + \hat{b}_{\text{out}}(t)] - i\epsilon [-\hat{a}_{\text{in}}(t) + \hat{a}_{\text{out}}(t)] \quad (\text{B19})$$

$$\epsilon = \frac{Z_0}{\omega_0 L_p} \quad (\text{B20})$$

$$\alpha = \frac{C_c}{C + 2C_c} \sqrt{\frac{Z_0}{Z_{LC}}} \sqrt{\omega_0} = \sqrt{\gamma}. \quad (\text{B21})$$

We can also express the out-fields as a function of in-fields

$$\hat{a}_{\text{out}}(t) = \alpha \hat{a}(t) - \frac{1}{1 + 2i\epsilon} \hat{a}_{\text{in}}(t) - \frac{2i\epsilon}{1 + 2i\epsilon} \hat{b}_{\text{in}}(t) \quad (\text{B22})$$

$$\hat{b}_{\text{out}}(t) = \alpha \hat{a}(t) - \frac{1}{1 + 2i\epsilon} \hat{b}_{\text{in}}(t) - \frac{2i\epsilon}{1 + 2i\epsilon} \hat{a}_{\text{in}}(t). \quad (\text{B23})$$

The Heisenberg equations of motion for the cavity are (under a rotating-wave approximation and using the new notation)

$$\begin{aligned} \hat{a}(t) &= -i\omega_0 \hat{a}(t) + \frac{\alpha}{2} [\hat{a}_{\text{in}} - \hat{a}_{\text{out}}] \\ &+ \frac{\alpha}{2} [\hat{b}_{\text{in}} - \hat{b}_{\text{out}}]. \end{aligned} \quad (\text{B24})$$

Inserting the solutions of Eqs. (B22-B23) in the cavity equation of motion we get

$$\hat{a}(t) = -i\omega_0 \hat{a}(t) - \alpha^2 \hat{a}(t) + \alpha [\hat{a}_{\text{in}}(t) + \hat{b}_{\text{in}}(t)]. \quad (\text{B25})$$

We obtain that (in the presence of the background) the equation of motion for the cavity remains unchanged, i.e., is independent of ϵ . The interference between propagation through the cavity and parallel inductor is described by Eqs. (B22-B23). These important results can be understood qualitatively as a consequence of that the reactive parallel element effectively only changes the phase of the drive, not its absolute value, and that this can be accounted for afterwards, without a change in the cavity equation of motion.

Appendix C: Fano curve tilt direction

An important detail is the tilt direction of the Fano curve, i.e., on which side of the resonance frequency is the minimum. The direction of the tilt is in our examples always rightwards. It is determined by two properties: (i) The change of the phase between the resonator input and output and (ii) the nature of the parallel coupling (capacitive or inductive).

In the case of a $\lambda/2$ -resonator the output and input fields are related at resonance as $b_{\text{out}}(\omega_0)/a_{\text{in}}(\omega_0) = (-1)^{n+1}$ for modes $n = 1, 2, \dots$. The first mode ($n = 1$) then keeps the sign and the second mode ($n = 2$) inverts the sign. The in-line resonator of Fig. 1(b) inverts the sign at the resonance and is then equivalent to $n = 2, 4, \dots$. In other words, the in-line resonator and coplanar resonator are equivalent for full-wavelength modes. However, we find that the model based on an in-line resonator can effectively describe also odd modes ($n = 1, 3, \dots$), if one makes a switch between an inductive and capacitive parallel coupling, i.e., changes the sign of ϵ . This is also the reason why our theoretical model considers explicitly a parallel inductor, but analysis of the experiment interprets the value of ϵ to originate from a parallel capacitor.